Inorganic Chemistry

Article

pubs.acs.org/IC

Coinage Metal Complexes Supported by the Tri- and Tetraphosphine Ligands

Minh Thuy Dau,[†] Julia R. Shakirova,[‡] Antti J. Karttunen,[§] Elena V. Grachova,*[,‡] Sergey P. Tunik,*[,‡] Alexey S. Melnikov,[∥] Tapani A. Pakkanen,[†] and Igor O. Koshevoy*[,†]

[†]Department of Chemistry, University of Eastern Finland, Joensuu, 80101, Finland

[‡]Department of Chemistry, St. Petersburg State University, Universitetskii pr. 26, 198504, St. Petersburg, Russia

[§]Department of Chemistry, Aalto University, FI-00076 Aalto, Finland

[∥]St. Petersburg State Polytechnical University, Polytechnicheskaya Str. 29, 195251 St. Petersburg, Russia

Supporting Information

ABSTRACT: A series of tri- and tetranuclear phosphine complexes of d^{10} metal ions supported by the polydentate ligands, bis(diphenylphosphinomethyl)phenylphosphine (*PPP*) and tris(diphenylphosphinomethyl)phosphine (*PPPP*), were synthesized. All the compounds under study, $[AuM_2(PPP)_2]^{3+}$ (M = Au (**1**), Cu (**2**), Ag (**3**)), $[M_4(PPPP)_2]^{4+}$ (M = Ag (**4**), Au (**5**)), $[AuAg_3(PPPP)_2]^{4+}$ (**6**), and $[Au_2Cu_2(PPPP)_2(NCMe)_4]^{4+}$ (**7**), were characterized crystallographically. The trinuclear clusters **1**−**3** contain a linear metal core, while in the isostructural tetranuclear complexes **4**−**6** the metal framework has a plane star-shaped arrangement. Cluster **7** adopts a structural motif that involves a digold unit bridged by two arms of the *PPPP* phosphines and decorated two spatially separated Cu^I ions chelated by the remaining P donors. The NMR spectroscopic investigation in DMSO solution revealed the heterometallic clusters **2**, **3**, and **6** are stereochemically nonrigid and undergo reversible metal ions redistribution between several species, accompanied by their solvation−desolvation. The complexes **1**−**3** and **5**−**7** exhibit room temperature luminescence in the solid state (Φ_{em} = 6−64%) in the spectral region from 450 to 563 nm. The phosphorescence observed originates from the triplet excited states, determined by the metal cluster-centered $d_{\sigma^*} \rightarrow p_\sigma$ transitions.

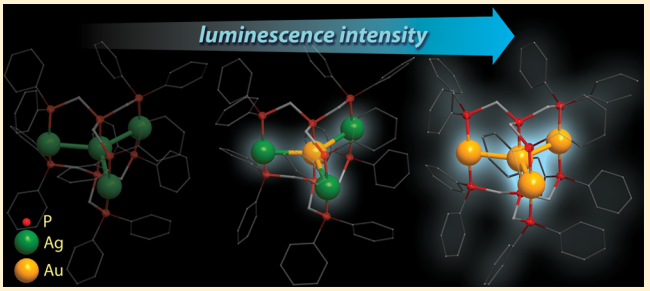

INTRODUCTION

Luminescence of copper subgroup metals coordination complexes and polymetallic clusters has considerably stimulated synthetic chemistry of these elements. It is reflected by the impressive progress in preparation of a wide variety of compounds of different nuclearity, which, in particular, exhibit attractive photophysical properties.[1] It is generally recognized that the metal−metal interactions, typically found among d^{10} ions of Cu^I, Ag^I, and Au^I, are one of the key factors influencing the energy and efficiency of emission of the polymetallic aggregates in the solid state and in solution.[1a,d,e,g,2] The cluster-centered electronic transitions, which are primarily responsible for the luminescence characteristics, strongly depend on geometry of a metal core, ligand environment, and the chemical nature of the constituting metal centers. Relatively low energies of the metal−metal contacts, comparable to those of hydrogen bonding, often make d^{10} clusters sensitive to subtle external changes (temperature,[2g,3] mechanical force,[4] guest ions,[5] volatile organics,[5d,6] etc.) resulting in visible alteration of absorption and emission properties that opens a way to selective and easy-to-detect sensing. Understanding the synergistic effects of the metal ions and the metal−metal interactions, influencing the emissive excited states, is important for the design of effective sensors and electroluminescent devices. Therefore, it is essential to carry out a systematic alteration of the metal framework preferably without other stereochemical variations within a family of congener complexes. However, preparation of a series of structurally similar compounds having different compositions of the homo- or heterometallic cluster core might be synthetically challenging due to the unequal coordination preference of the metal ions, even of those belonging to same group.

The clusters of small nuclearity (M_n, n = 2−4) are the attractive model candidates to study the effect of the composition of the metal core on the photophysical characteristics within the series of isostructural species. In particular, their similarity may allow for approximately the same contribution of the ligands' orbitals to the excited states of the clusters, and the observed differences in spectroscopic behavior can be attributed mainly to the changes in the metal framework. Interestingly, among the d^{10} coinage metals, the heterotrinuclear systems of M−M′−M type are extremely rare

Received: February 19, 2014
Published: April 21, 2014

   dx.doi.org/10.1021/ic500402m | *Inorg. Chem.* 2014, 53, 4705−4715

with only one Cu−Au−Cu example bearing pyridyl-carbene ligands.[6a]

Inspired by the literature reports on bright luminescence of the homometallic linear Au_n and Ag_n (n = 3, 4) tri- and tetraphosphine complexes, which show quantum yields reaching 97% at room temperature,[1t,7] we attempted to synthesize the heterometallic d^{10} analogues M−M′−M supported by the analogous triphosphine ligand and to extend these studies to the tetranuclear complexes based on the C_3-symmetrical tetraphosphine (Figure 1) that has not been used yet in coordination chemistry of coinage metals.

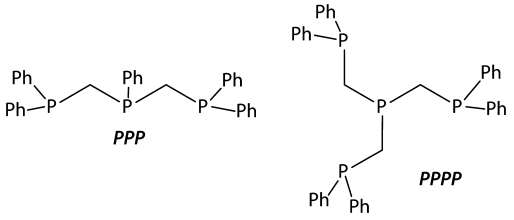

Figure 1. Phosphine ligands used in the current work.

EXPERIMENTAL SECTION

General Comments. The ligands bis(diphenyl-phosphinomethyl)-phenylphosphine (*PPP*), tris(diphenyl-phosphinomethyl)phosphine (*PPPP*),[8] and the complex AuCl(tht) (tht = tetrahydrothiphene)[9] were synthesized according to the published procedures. Other reagents and solvents were used as received. Solution ^{1}H and ^{31}P{^{1}H} NMR spectra were recorded by a Bruker Avance 400 spectrometer. Microcrystalline powders were used as assays for photophysical experiments. Absorption spectra were recorded using a Lambda 1050 spectrophotometer; excitation and emission spectra were measured on a Fluorolog 3 spectrofluorimeter. Life time was measured and calculated by the TCSPC (Time-Correlated Single Photon Counting) method. The integration sphere was used to measure the solid state emission quantum yield for the complexes tableted with KBr. Microanalyses were carried out in the analytical laboratory of the University of Eastern Finland.

$[Au_3(PPh_2CH_2PPhCH_2PPh_2)_2](PF_6)_3$ ***(1)***. AuCl(tht) (500 mg, 1.56 mmol) was dissolved in dichloromethane (15 cm^3), and *PPP* (525 mg, 1.04 mmol) was added, followed by a solution of $AgPF_6$ (395 mg, 1.56 mmol) in acetone (5 cm^3). Upon the addition of $AgPF_6$, a flaky precipitate of AgCl gradually formed. The reaction mixture was stirred for an additional 30 min in the absence of light. AgCl was removed by filtration; the colorless solution was passed through a layer of silica gel and evaporated. Colorless amorphous residue was thoroughly washed with diethyl ether and recrystallized by gas-phase diffusion of diethyl ether into an acetone/methanol solution of **1** (5:1 v/v mixture) at 278 K to give colorless crystalline material (943 mg, 89%). Anal. Calcd for $Au_3C_{64}H_{58}P_9F_{18}$: C, 37.70%; H, 2.87%. Found: C, 37.69%; H, 2.98%. ^{31}P{^{1}H} NMR (DMSO-d_6, RT; δ): A_2B_4 system, 34.9 (m, 4P, $P^{lateral}$–Au), 31.8 (m, 2P, $P^{central}$–Au), −144.2 (sept, 3P, PF_6^-). ^{1}H NMR (DMSO-d_6, RT; δ): 7.96 (m, 8H, J_{PH} = 14.5 Hz, J_{HH} = 7.6 Hz, *ortho*-H C_6H_5), 7.70 (m, 4H, J_{PH} = 13.4, Hz, J_{HH} = 7.3 Hz, *ortho*-H C_6H_5), 7.69 (m, 12H, J_{HH} ∼ 7 Hz, AB_2 system of *meta*-H + *para*-H C_6H_5), 7.69 (m, 8H, J_{PH} = 13.4 Hz, J_{HH} = 7.8 Hz, *ortho*-H C_6H_5), 7.46 (t, 4H, J_{HH} = 7.8 Hz, *para*-H C_6H_5), 7.44 (p, 2H, J_{HH} = 7.3 Hz, *para*-H C_6H_5), 7.33 (dd, 8H, J_{HH} = 7.8 Hz, *meta*-H), 7.24 (dd, 4H, J_{HH} = 7.3 Hz, *meta*-H), 4.93 (m, 4H, CH_2), 4.02 (m, 4H, CH_2).

$[AuCu_2(PPh_2CH_2PPhCH_2PPh_2)_2](PF_6)_3$ ***(2)***. AuCl(tht) (50 mg, 0.156 mmol) was dissolved in dichloromethane (7 cm^3), and tht (2 drops) was added, followed by a solution of $AgPF_6$ (40 mg, 0.158 mmol) in acetone (3 cm^3). The reaction mixture was stirred for 30 min in the absence of light. AgCl was removed by filtration, and crystalline *PPP* (159 mg, 0.314 mmol) was added to the resulting colorless solution. After the triphosphine dissolved, the mixture was evaporated, and the solid residue was washed with diethyl ether (3 × 5 cm^3). Then the solid was dissolved in dichloromethane (5 cm^3) and treated with a solution of solution of $Cu(NCMe)_4PF_6$ (117 mg, 0.314 mmol) in the same solvent (5 cm^3). Pale yellow solution was stirred for 1 h and evaporated, and the amorphous solid was recrystallized by gas-phase diffusion of diethyl ether into a dichloromethane/methanol solution of **2** at 278 K, giving pale yellow crystalline material (221 mg, 80%). Anal. Calcd for $C_{64}H_{58}AuCu_2F_{18}P_9$: C, 43.38%; H, 3.30%. Found: C, 43.24%; H, 3.36%. ^{31}P{^{1}H} NMR (DMSO-d_6, RT; δ): A_2X_4 system, J_{AA} = 320 Hz, J_{XX} = 100 Hz, J_{AX} = 93 Hz; 34.0 (m, 2P, P−Au), −8.7 (broad m, 4P, P−Cu), −144.2 (sept, 3P PF_6^-).

$[AuAg_2(PPh_2CH_2PPhCH_2PPh_2)_2](PF_6)_3/(ClO_4)_3$ ***(3a/b)***. Compounds **3a** and **3b** were prepared similarly to **2** starting from AuCl(tht) (35 mg, 0.109 mmol), *PPP* (111 mg, 0.219 mmol), and stoichiometric amounts of the corresponding silver salt, $AgPF_6$ (56 mg, 0.221 mmol) or $AgClO_4$ (56 mg, 0.221 mmol). Recrystallization by gas-phase diffusion of diethyl ether into dichloromethane/methanol (**3a**) or acetonitrile/methanol (**3b**) solution at 278 K gave colorless crystalline material (**3a**: 148 mg, 73%; **3b**: 154 mg, 82%). Anal. Calcd for **3a**, $C_{64}H_{58}Ag_2AuF_{18}P_9$: C, 41.31%; H, 3.14%. Found: C, 41.14%; H, 3.40%. Anal. Calcd for **3b** $C_{64}H_{58}Ag_2AuCl_3O_{12}P_6$: C, 44.59%; H, 3.39%. Found: C, 44.45%; H, 3.43%. The NMR spectroscopic parameters of **3a** and **3b** are virtually identical. ^{31}P{^{1}H} NMR (DMSO-d_6, RT; δ): $A_2X_4Q_2$ system, J_{AA} = 320 Hz, J_{XX} = 100 Hz, J_{AX} = 106 Hz, J^{109}_{AgP} = 550 Hz, J^{107}_{AgP} = 466 Hz; ***nonsolvated complex***: 38.2 (m, 2P, P−Au), 4.8 (dm, 4P, P−Ag); ***DMSO solvate***: 36.1 (m, 2P, P−Au), 3.9 (dm, 4P, P−Ag).

$[Ag_4\{(PPh_2CH_2)_3P\}_2](ClO_4)_4$ ***(4)***. $AgClO_4$ (75 mg, 0.361 mmol) was dissolved in methanol (4 cm^3) and added to a solution of *PPPP* (114 mg, 0.182 mmol) in dichloromethane (10 cm^3). Colorless transparent solution was stirred for 30 min in the absence of light and evaporated. Amorphous solid was washed with diethyl ether (3 × 5 cm^3) and recrystallized by gas-phase diffusion of diethyl ether into an acetonitrile/methanol solution of **4** at 278 K to give colorless crystalline material (170 mg, 90%). Anal. Calcd for $C_{78}H_{72}Ag_4Cl_4O_{16}P_8$: C, 44.90%; H, 3.48%. Found: C, 44.99%; H, 3.73%. ^{31}P{^{1}H} NMR (DMSO-d_6, RT; δ): $A_2X_6PQ_3$ system, J_{AX} = 140 Hz; 14.9 (dm, 2P, J^{109}_{AgP} = 548 Hz, J^{107}_{AgP} = 474 Hz, $P^{central}$–Ag), 2.9 (dm, 6P, $J109_{AgP}$ = 567 Hz, $J107_{AgP}$ = 486 Hz, $P^{lateral}$–Ag). ^{1}H NMR (DMSO-d_6, RT; δ): 7.80 (m, 24H, *ortho*-H, C_6H_5), 7.64 (m, 36H, *meta*-H + *para*-H, C_6H_5), 3.08 (broad, 12H, CH_2).

$[Au_4\{(PPh_2CH_2)_3P\}_2](PF_6)_4$ ***(5)***. Compound **5** was prepared similarly to **1** starting from AuCl(tht) (150 mg, 0.468 mmol), *PPPP* (147 mg, 0.234 mmol), and $AgPF_6$ (119 mg, 0.470 mmol). Recrystallization by gas-phase diffusion of diethyl ether into an acetonitrile/dichloromethane solution of **5** at 278 K gave colorless crystalline material (240 mg, 78%). Anal. Calcd for $C_{78}H_{72}Au_4F_{24}P_{12}$: C, 35.69%; H, 2.77%. Found: C, 35.98%; H, 2.97%. ^{31}P{^{1}H} NMR (DMSO-d_6, RT; δ): A_2B_6 system, 32.4 (m, 6P, $P^{lateral}$–Au), 31.5 (m, 2P, $P^{central}$–Au), −144.2 (sept, 4P, PF_6^-). ^{1}H NMR (DMSO-d_6, RT; δ): 7.95 (m, 24H, J_{HH} = 6.0 Hz, J_{PH} = 12.7 Hz, *ortho*-H, C_6H_5), 7.69 (m, 36H, J_{HH} ∼ 7.0 Hz, AB_2 system of *meta*-H + *para*-H, C_6H_5), 3.82 (broad, 12H, CH_2).

$[AuAg_3\{(PPh_2CH_2)_3P\}_2](ClO_4)_4$ ***(6)***. Compound **6** was prepared similarly to **3** starting from AuCl(tht) (40 mg, 0.125 mmol), *PPPP* (157 mg, 0.25 mmol) and stoichiometric amounts of $AgClO_4$. Recrystallization by gas-phase diffusion of diethyl ether into an acetonitrile solution of **6** at 278 K gave colorless crystalline material (214 mg, 79%). Anal. Calcd for $C_{78}H_{72}Ag_3AuCl_4O_{16}P_8$: C, 43.06%; H, 3.34%. Found: C, 42.85%; H, 3.59%. ^{31}P{^{1}H} NMR (DMSO-d_6, RT; δ): $A_2X_6Q_3$ system, J_{AA} = 295 Hz, J_{XX} = 95 Hz, J_{AX} = 102 Hz; 38.2 (m, 2P, P−Au), −0.5 (dm, 6P, J^{109}_{AgP} = 560 Hz, J^{107}_{AgP} = 475 Hz, P−Ag).

$[Au_2Cu_2\{(PPh_2CH_2)_3P\}_2(NCMe)_2](PF_6)_4$ ***(7)***. AuCl(tht) (75 mg, 0.234 mmol) was dissolved in dichloromethane (7 cm^3), and tht (2 drops) was added, followed by a solution of $AgPF_6$ (60 mg, 0.237 mmol) in acetone (4 cm^3). The reaction mixture was stirred for 30 min in the absence of light. AgCl was removed by filtration, and *PPPP* (147 mg, 0.234 mmol) was added to the resulting colorless solution. After stirring for an additional 30 min, the solvents were evaporated, and the residue was dried thoroughly under a vacuum to remove the excess of tht. Then, it was dissolved in dichloromethane (10 cm^3), and a

dx.doi.org/10.1021/ic500402m | Inorg. Chem. 2014, 53, 4705−4715

Scheme 1. Synthesis of the Clusters 1−3

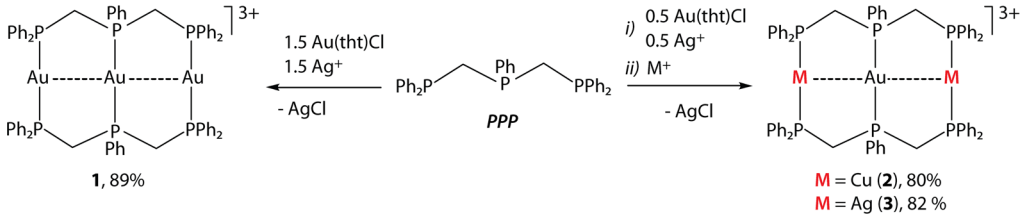

solution of $Cu(NCMe)_4PF_6$ (88 mg, 0.236 mmol) in dichloromethane (5 cm^3) was added. The pale yellow opaque mixture was stirred overnight, filtered, evaporated, and recrystallized by gas-phase diffusion of diethyl ether into acetonitrile/methanol solution of **7** at 278 K to give pale yellow crystalline material (238 mg, 81%). Anal. Calcd for $C_{86}H_{84}Au_2Cu_2F_{24}N_4P_{12}$: C, 40.95%; H, 3.36%; N, 2.22%. Found: C, 40.97%; H, 3.39%; N, 2.20%. $^{31}P\{^1H\}$ NMR (DMSO-d_6, RT; δ): $A_2X_2Q_4$ system, J_{A-Au-X} = 320 Hz, J_{AX} = 45 Hz, J_{AQ} = 45 Hz; 33.6 (dd, 2P, $P^{lateral}$−Au), 16.3 (ddt, 2P, $P^{central}$−Au), −24.7 (broad m, 4P, $P^{lateral}$−Cu), −144.6 (sept, 4P, PF_6^-). ^1H NMR (DMSO-d_6, RT; δ): 7.88 (t, 4H, J_{HH} = 7.6 Hz, *para*-H C_6H_5), 7.80 (dd, 8H, J_{HH} = 7.6 Hz, *meta*-H C_6H_5), 7.56 (m, 8H, J_{PH} = 11.5 Hz, J_{HH} = 7.2 Hz, *ortho*-H C_6H_5), 7.51 (m, 12H, J_{HH} ∼ 7 Hz, AB_2 system of *meta*-H + *para*-H C_6H_5), 7.28 (m, 8H, J_{HH} = 7.2 Hz, J_{PH} = 13.6 Hz, *ortho*-H C_6H_5), 7.27 (m, 8H, J_{HH} = 7.6 Hz, J_{PH} = 14.1 Hz, *ortho*-H C_6H_5), 7.15 (m, 12H, J_{HH} ∼ 7 Hz, AB_2 system of *meta*-H + *para*-H C_6H_5), 3.94 (m, 8H, CH_2), 2.81 (m, 4H, CH_2), 2.09 (s, 12H, NCMe).

Computational Details. The clusters **1**−**7** were studied using a hybrid PBE0 density functional method.[10] The copper, silver, and gold atoms were described by a triple-ζ-valence quality basis set with polarization functions (def2-TZVP).[11] Scalar relativistic effects were taken into account by applying 28- and 60-electron relativistic effective core potentials for Ag and Au, respectively.[12] A split-valence basis set with polarization functions on non-hydrogen atoms was used for all the other atoms.[13] To facilitate comparisons with the experiments, point group symmetry was applied as follows: **1**, **3a**: C_{2h}; **2**: C_i, **3b**: C_{2v}, **4**−**6**: C_{3h}, **7**: C_i. The geometries of all complexes were fully optimized. The excited states were investigated with the time-dependent DFT approach.[14] The singlet excitations were determined at the optimized ground state S_0 geometries, while the lowest energy triplet emissions were determined at the optimized T_1 geometry. All electronic structure calculations were carried out with the TURBOMOLE program package (version 6.5).[15]

X-Ray Structural Determination. The crystals of **1**−**7** were immersed in cryo-oil, mounted in a Nylon loop, and measured at a temperature of 120 K. The X-ray diffraction data were collected on a Bruker SMART APEX II diffractometer using Mo Kα radiation (λ = 0.71073 Å). The *APEX2*[16] program package was used for cell refinements and data reductions. The structures were solved by direct methods using the *SHELXS-97*[17] programs with the *WinGX*[18] graphical user interface. A semiempirical absorption correction (*SADABS*)[19] was applied to all data. Structural refinements were carried out using *SHELXL-97* and *SHELXL-2013*.[17]

The crystallization acetone (in **1**) and acetonitrile (in **3b**) molecules were partially lost and therefore were refined with occupancies of 0.5. Both geometrical and displacement constraints and restraints were applied to these moieties.

Some of the dichloromethane (in **2**, **3a**, **5**), diethyl ether (in **2**), acetonitrile (in **4**, **5**, **7**), and methanol (**7**) crystallization molecules were disordered over two sites each and were refined with occupancies, CH_2Cl_2: 0.78/0.22 (**2**), 0.50/0.50 (**3a**), 0.70/0.30 (**5**); Et_2O: 0.57/0.43 (**2**); NCMe: 0.53/0.47 (**4**), 0.50/0.50 (**5**), 0.55/0.45 (**7**); MeOH: 0.58/0.42 (**7**). A series of geometrical restraints were applied to these disordered moieties (in **2**, **4**, **5**, **7**).

One of the phenyl rings in **3b** was disordered over two positions (C57−C62, C157−C162) and was refined with occupancies 0.63/0.37. The displacement parameters of the carbon atoms of both components were constrained to be equal within each group. The aromatic ring C157−C162 was geometrically idealized.

In **5**, a disorder model involving the phenyl ring (C37−C42) and crystallization molecules of dichloromethane (Cl3, Cl4, C83), acetonitrile (N5, C89, C90), and diethyl ether (C94−C97, O1) was built, and the components were refined with occupancies 0.58/0.42. The aromatic ring was geometrically idealized. A series of geometrical and displacement restraints and constraints were applied to the solvent molecules.

Some of the solvent molecules in the unit cells of **6** were omitted as they could not been resolved unambiguously. The missing solvent was taken into account by using a *SQUEEZE* routine of *PLATON*[20] and was not included into the cell content.

One PF_6^- counterion in **1** was disordered over two equivalent positions (P7, F7−F12). A series of geometric and displacement constraints and restraints were applied to both components. The displacement parameters of the fluorine atoms were constrained to be equal.

The silver atoms (Ag1 in **3a**; Ag1 and Ag2 in **3b**) were found in two sites and were refined with occupancies 0.80/0.20 (**3a**) and 0.62/0.38 and 0.94/0.06 (**3b**). The displacement parameters within each disordered moiety were constrained to be equal.

The idealized positions of the hydrogen atoms of the water molecule in **2** and **3a** were estimated with the *HYDROGEN*[21] program and constrained to ride on their parent atom with U_{iso} = 1.5 U_{eq} (parent atom). The methanol OH hydrogen atom in **3b** was positioned manually and was constrained to ride on its parent atom with U_{iso} = 1.5 U_{eq} (parent atom). All hydrogen atoms in **1**−**7** were positioned geometrically and constrained to ride on their parent atoms with C−H = 0.95−0.99 Å and U_{iso} = 1.2−1.5 U_{eq} (parent atom). The crystallographic details are summarized in Table S1.

RESULTS AND DISCUSSION

Synthesis and Structural Characterization. *Trinuclear Complexes.* Formation of the trimetallic compounds $[M_3(PPP)_2]^{3+}$ (M = Ag, Au) can be easily achieved by reacting the corresponding metal salts with a stoichiometric amount of the triphosphine ligand followed by the subsequent exchange of counterions in the case of Au^I.[7] Synthesis of $[Au_3(PPP)_2](PF_6)_3$ (**1**) herein was carried out using a slightly modified procedure (Scheme 1).[7b]

The preparation of the heterometallic compounds followed the same general strategy and involved reaction of the AuCl(tht) (tht = tetrahydrothiophene) precursor with 2 equiv of the triphosphine, removal of the chlorides with Ag^+, and addition of the needful amount of M^+ ions to give the $[M_2Au(PPP)_2]^{3+}$ clusters, M = Cu (**2**), Ag (**3**), as air and moisture stable solids after the recrystallization.

The structures of **1**−**3** were estimated by X-ray crystallographic study. The trinuclear complex **1** has a linear arrangement of metal centers (Au(1)−Au(2)−Au(1′) angle is 180°), which are held together by two bridging triphosphines. **1** is isostructural to its close congener bearing P ligands with cyclohexyl substituents (Figure S1, Supporting Information).[7b] The analogue of **1** with SCN^- counterions[22] has a more bent geometry with a Au−Au−Au angle of 167.2°. The complexes **2** and **3a**, which were isolated as PF_6^- salts, were found to be isomorphic as they crystallize in the same type of a spacegroup

dx.doi.org/10.1021/ic500402m | Inorg. Chem. 2014, 53, 4705−4715

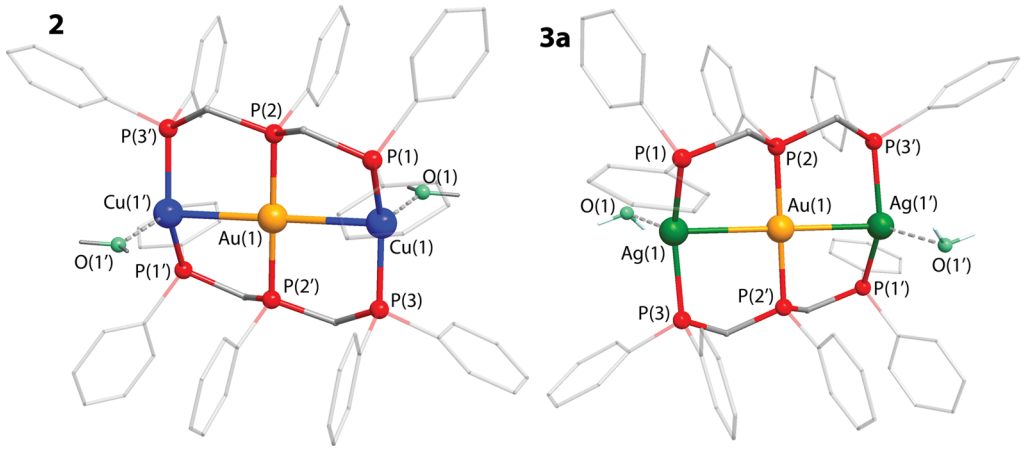

Figure 2. Molecular views of the trications **2** and **3a**. Symmetry transformations used to generate equivalent atoms (′) in **2**: 2 − *x*, 1 − *y*, −*z*; in **3a**: 1 − *x*, 1 − *y*, 1 − *z*.

Table 1. Selected Bond Lengths and Angles for Complexes 1, 2, and 3a

	1 (M = Au)	**2** (M = Cu)	**3a** (M = Ag)[a]
	bond lengths, Å		
Au(1)−M(1)	2.92431(15)[b]	2.9042(3)	3.0138(4)
P(1)−M(1)	2.3142(10)	2.2615(7)	2.4187(8)
P(2)−Au(1)	2.3180(9)[b]	2.3041(6)	2.3234(7)
P(3)−M(1)	2.3178(10)	2.2723(7)	2.4463(9)
O(1)−M(1)		2.136(2)	2.403(3)
	bond angles, deg.		
P(2)−Au(1)−P(2′)	180.00(5)[b]	180	180
P(1)−M(1)−P(3)	175.26(3)[b]	144.92(3)	143.14(5)
M(1)−Au(1)−M(1′)	180[b]	180	180

[a]The structural parameters are given for the major component of the disordered molecule. [b]M(1) = Au(1), Au(1) = Au(2).

Scheme 2. Synthesis of the clusters 4−7

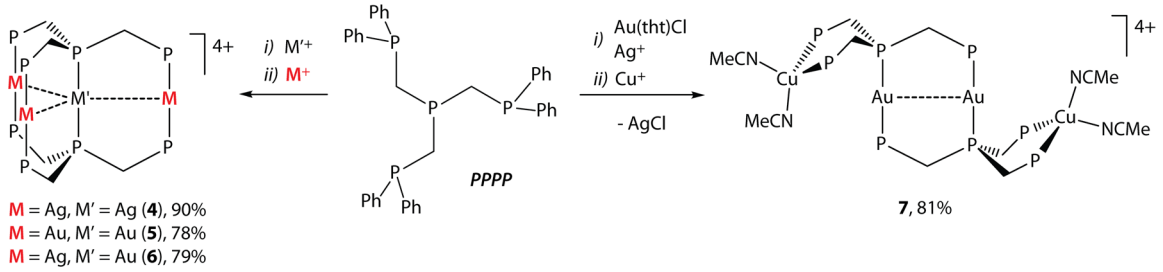

($P\bar{1}$) and have very close parameters of the unit cells (Table S1). Similarly to **1**, the bimetallic compounds as well possess linear metal-triphosphine frameworks (Figure 2, an ORTEP view is shown in Figure S1, selected structural parameters are listed in Table 1). The M−Au−M chains are supported by the *PPP* ligands with gold atoms occupying the central position in both clusters. In both trications **2** and **3a**, the angle M−Au−M is 180°. The metal−metal distances in **2** (2.9042 Å) and in **3** (2.998 and 3.0138 Å) are considerably shorter than the sum of the corresponding van der Waals radii (3.06 Å for Cu−Au and 3.38 Å for Ag−Au) that points to the presence of appreciable metallophilic interactions. Both **2** and **3a** were found as solvates, having water molecules attached to each of the terminal Cu or Ag atoms. The O−Ag distance (2.403 Å) is significantly smaller than the O−Cu contact (2.136 Å). The silver atoms in **3a** are disordered and the minor component; the O···Ag(11) separation of 2.831 Å indicates a much weaker metal−ligand bonding interaction. The presence of coordinated water molecules probably determines the distortions of coordination geometry of copper and silver ions from the linear one (the angles P−M−P are 144.9° in **2** and 143.1° in **3a**).

The nature of crystallization solvent/counterions thus could lead to the distortions of the metal core in this type of compounds. Indeed, crystallization of the Au−Ag cluster as ClO_4^- salt in the presence of acetonitrile gave the modification **3b** (Figure S1). As in **3a**, the Ag ions are disordered and occupy two positions each. The major component of the disordered molecule has two acetonitrile ligands coordinated to both silver centers. Additionally, in **3b** the metal core is bent with the Ag−Au−Ag angle being 163.14° (cf. 180° in **3a**), while the metal−metal contacts (3.033 and 3.037 Å) and the P−Ag−P angles (139.0 and 146.8°) are close to the corresponding values found in **3a**. The close congener of **3b**, the trisilver cluster

dx.doi.org/10.1021/ic500402m | *Inorg. Chem.* 2014, 53, 4705−4715

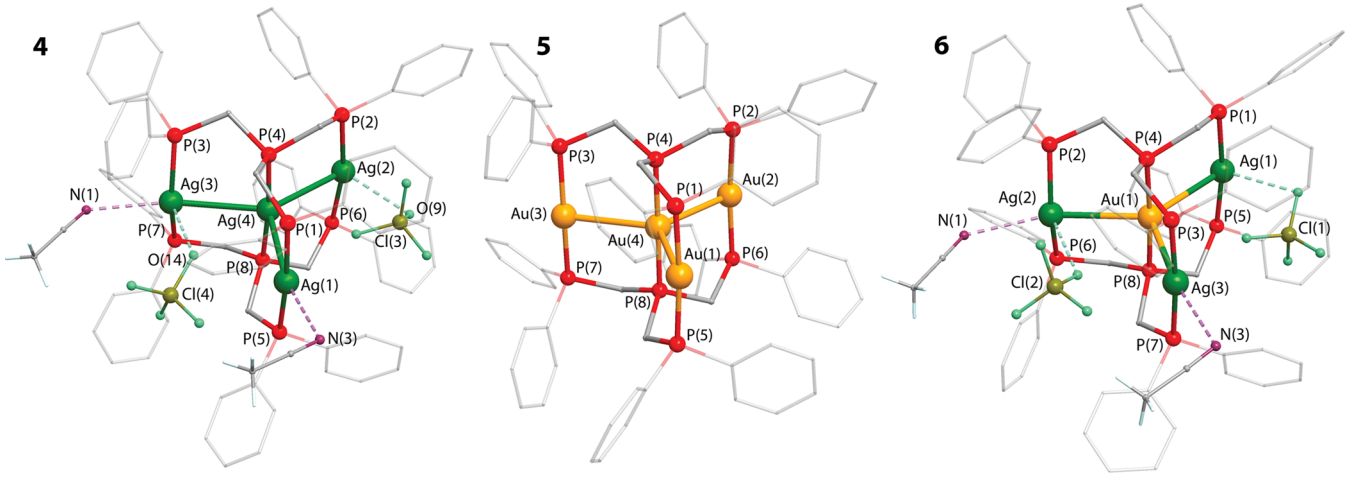

Figure 3. Molecular views of the tetracations **4**–**6**. Only the counterions and solvent molecules interacting with metal ions are shown.

Table 2. Selected Bond Lengths and Angles for Complexes 4–6

	4 (M = Ag)	**5** (M = Au)		**6**
		bond lengths, Å		
M(1)–M(4)	3.1303(6)	3.0071(3)	Ag(1)–Au(1)	3.1475(6)
M(2)–M(4)	3.1568(6)	3.0297(3)	Ag(2)–Au(1)	3.1058(7)
M(3)–M(4)	3.1540(6)	3.0146(3)	Ag(3)–Au(1)	3.1136(8)
P(1)–M(1)	2.4603(16)	2.3135(13)	P(1)–Ag(1)	2.398(2)
P(2)–M(2)	2.4327(15)	2.3141(13)	P(2)–Ag(2)	2.416(2)
P(3)–M(3)	2.4409(15)	2.3099(14)	P(3)–Ag(3)	2.446(2)
P(4)–M(4)	2.3599(14)	2.2850(13)	P(4)–Au(1)	2.3152(18)
P(5)–M(1)	2.4528(16)	2.3124(13)	P(5)–Ag(1)	2.400(2)
P(6)–M(2)	2.4255(15)	2.3141(14)	P(6)–Ag(2)	2.424(2)
P(7)–M(3)	2.4340(15)	2.3118(14)	P(7)–Ag(3)	2.447(2)
P(8)–M(4)	2.3570(14)	2.2833(13)	P(8)–Au(1)	2.3151(18)
		bond angles, deg.		
P(1)–M(1)–P(5)	174.33(6)	174.57(5)	P(1)–Ag(1)–P(5)	172.78(8)
P(2)–M(2)–P(6)	169.71(5)	175.27(5)	P(2)–Ag(2)–P(6)	153.17(8)
P(3)–M(3)–P(7)	152.51(5)	172.09(5)	P(3)–Ag(3)–P(7)	174.59(8)
P(4)–M(4)–P(8)	175.23(5)	179.25(5)	P(4)–Au(1)–P(8)	176.87(8)

$[Ag_3(PPP)_2](ClO_4)_3$, shows very similar deviations from the linearity of the side Ag atoms (the values of P–Ag–P angles are 161.2° and 137.9°), that can be also attributed to the presence of coordinated acetonitrile molecules.[7a] Additionally, the Ag(2)–O(1) separation of 2.871Å indicates weak cation··· anion bonding between the ClO_4^- anion and the lateral Ag center.

It should be noted that the solvent molecules in **2** and **3** are weakly coordinated and can be effectively removed from the crystalline samples under a vacuum as indicated by the results of elemental analyses (see Experimental Section).

It is worth mentioning that we attempted to synthesize the dinuclear Au–Cu and Au–Ag heterometallic complexes using the bridging diphosphine ligand, bis(diphenylphosphino)-methane (dppm). However, only the mixtures containing $[Au_2(dppm)_2]^{2+}$ and the related copper or silver compounds were obtained.

Tetranuclear Complexes. The preparation of the tetranuclear clusters was carried out according to the approach described for complexes **1**–**3**, using the branched C_3 symmetrical tetraphosphine ligand (Scheme 2). Thus, treatment of $AgClO_4$ or AuCl(tht) (in the presence of Ag^+) with 0.5 equiv of *PPPP* expectedly gave the homometallic species $[M_4(PPPP)_2]^{4+}$, M = Ag (**4**), Au (**5**) in good yields.

Sequential addition of Au^+ ions (generated *in situ* reacting the mixture {Au(tht)Cl + tht} with Ag^+) and Ag^+ to the tetraphosphine allowed for the isolation of a heterometallic complex $[AuAg_3(PPPP)_2]^{4+}$ (**6**) that is isostructural to **4** and **5**. However, following this methodology the reaction involving Cu^+ instead of Ag^+ resulted in formation of a tetranuclear Au–Cu cluster $[Au_2Cu_2(PPPP)_2(NCMe)_4]^{4+}$ (**7**) of a different structural type (Scheme 2), which was obtained in a good yield after optimizing the reaction stoichiometry. The Au–Ag analogue of **7** was not isolated even when a suitable ratio of the starting reagents was used.

The structures of **4**–**7** have been determined by XRD analysis. In congener complexes **4**–**6**, all the metal atoms lie approximately in one plane, three of which occupy the corners of an equilateral triangle, and the fourth one is located in its middle (Figures 3 and S2, selected structural parameters are listed in Table 2). The arrangement of the d^{10} ions is determined by the geometry of two *PPPP* ligands, which support the cluster framework. The values of metal–metal distances in **4**–**6** are typical for the corresponding Ag–Ag, Au–

dx.doi.org/10.1021/ic500402m | *Inorg. Chem.* 2014, 53, 4705–4715

Au, and Au−Ag metallophilic interactions reported in the literature.[7,23]

As in the case of **2** and **3a** clusters, the ClO_4^- salts of silver-containing complexes **4** and **6** are isomorphic (both were found in the spacegroup $Pna2_1$ and have nearly identical unit cell dimensions, Table S1).

These tetranuclear compounds have virtually the same arrangement of acetonitrile crystallization molecules weakly bound to the Ag ions in a manner found in **3b** and in $[Ag_3(PPP)_2](ClO_4)_3$.[7a] Similarly to **3b**, the acetonitrile ligands in **4** and **6** can easily dissociate giving solvent-free crystalline materials upon vacuum drying. The weak interactions of the ClO_4^- counterions with silver ions in **4** and **6** as well are very much alike and resemble the analogous contacts found in **3b** (Figure 3). Despite these very small crystallographic differences found in the solid samples of clusters **4** and **6**, the clear distinction of their photophysical behavior (see below) undoubtedly proves different compositions of the metal cores in these complexes.

The cluster **7** has the same nuclearity as the complexes **4**−**6** but adopts another structural motif (Figures 4 and S2). It

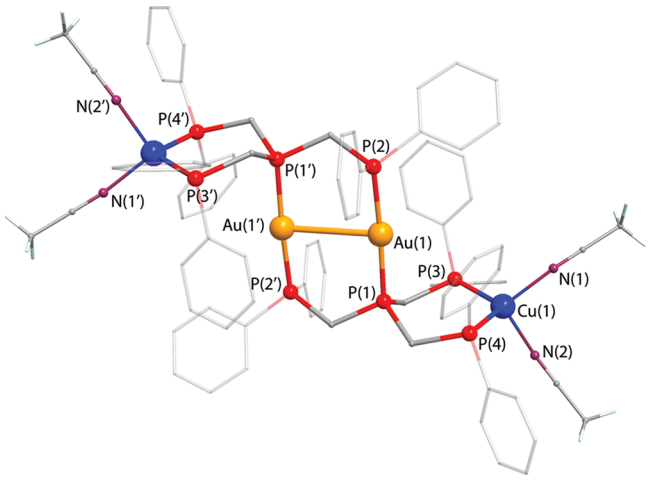

Figure 4. Molecular view of the tetracation **7**. One of the independent molecules found in the unit cell is shown. Selected interatomic distances (Å) are Au(1)−Au(1′) 3.1837(3), P(1)−Au(1) 2.3104(11), P(2)−Au(1) 2.3207(11), P(3)−Cu(1) 2.2410(13), P(4)−Cu(1) 2.2542(13), Cu(1)−N(1) 2.008(4), Cu(1)−N(2) 2.007(5). Symmetry transformations used to generate equivalent atoms (′) in **7**: $1 - x$, $1 - y$, $2 - z$.

contains a digold unit bridged by two arms of the *PPPP* phosphines and reminds one of a Au^I dimer supported by the dppm ligand, $[Au(dppm)_2]^{2+}$.[24] The remaining P donors of each tetraphosphine chelate two Cu^I ions. Coordination of two acetonitrile ligands to each of the copper centers completes the tetrahedral geometry around these metals. The long separations between gold and copper atoms exceeding 4.7 Å indicate an absence of any Au−Cu interactions.

Solution Behavior. *Trinuclear Complexes 1*−*3.* The ^{31}P and ^1H NMR spectroscopic measurements in DMSO-d_6 solution showed that complex **1** retains its structural motif found in the solid state. However, the heterometallic compounds **2** and **3** display metal ion migration between different phosphorus atoms of the polydentate ligands, whereas complex **3** also shows coordinated solvent dissociation to give presumably solvent-free and DMSO substituted forms, see below.

The homometallic $[Au_3(PPP)_2]^{3+}$ complex (**1**) gives two major signals (2:1 integral ratio) in the ^{31}P NMR spectrum (see Experimental Section and Figure S3), which can be considered as a strongly coupled A_2B_4 pattern that fits well the symmetry of this molecule and coupling network between the phosphorus nuclei. The appearance of a set of the minor resonances with chemical shifts close to those of the major signals (Figure S3) is tentatively assigned to the presence of an equilibrium involving the solvated and nonsolvated forms of the Au_3 cluster.

As mentioned above, **2** displays dynamic equilibrium between the species of different symmetry and different composition of the metal core due to migratory Cu↔Au ion exchange between central and lateral positions in the structure shown in Figure 2. The 1D ^{31}P and ^{31}P–^{31}P COSY NMR spectra of this compound are given in Figures 5 and S4 and allow for the complete assignment of the spectroscopic patterns to the possible forms of **2** existing in solution.

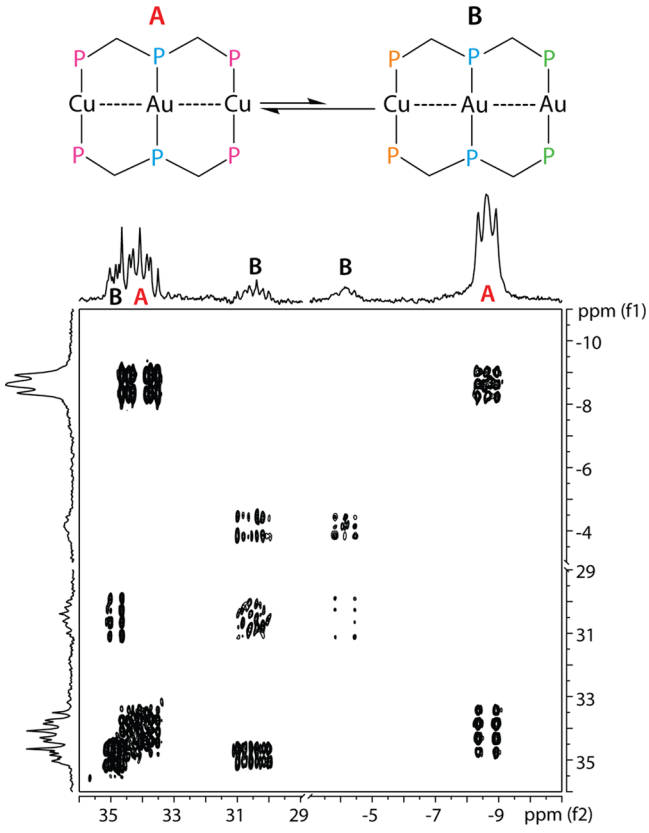

Figure 5. Scheme of the metal ion migration in **2** (top) and ^{31}P–^{31}P COSY NMR spectrum of **2**, DMSO-d_6, 298 K (bottom).

The major symmetrical $[AuCu_2(PPP)_2]^{3+}$ complex gives two resonances (34.0 ppm and −8.7 ppm, 1:2 intensity ratio), which can be easily simulated using the A_2X_4 coupling network as depicted in Figure S4, whereas the minor group of three multiplets (34.8 ppm, 30.3 ppm and −4.2 ppm, 1:1:1 intensity ratio) clearly correlated in the COSY spectrum may be ascribed to the asymmetric species of the $[Au_2Cu(PPP)_2]^{3+}$ type shown in Figure 5 (top). The possible formation of the species of general composition $[Cu_3(PPP)_2]^{3+}$ (necessary to keep the overall stoichiometry confirmed by elemental analysis) might not be detected due to a considerable fluxionality of the copper

dx.doi.org/10.1021/ic500402m | *Inorg. Chem.* 2014, 53, 4705−4715

compounds and their relatively low concentration. Moreover, the complex $[Cu_3(PPP)_2]^{3+}$ is not reported in the literature, and our attempts to prepare it were not successful giving few broad unresolved resonances of low intensity that probably indicates the formation of few stereochemically nonrigid species.

The crystalline sample of **3** in DMSO-d_6 gives the spectroscopic pattern, which consists of three groups of signals correlated in the $^{31}P-^{31}P$ COSY NMR spectrum, see Figure 6.

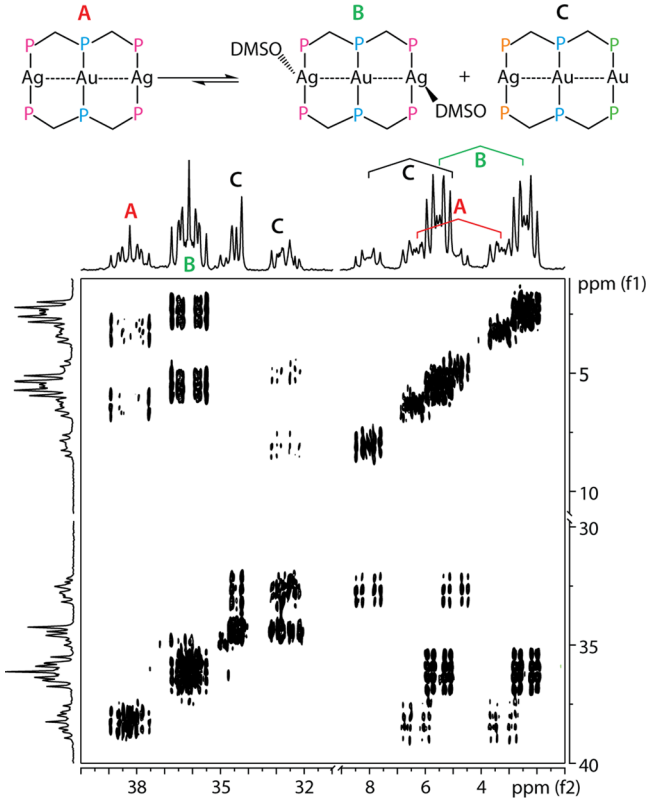

Figure 6. Scheme of the solvate forms equilibrium in **3** (top) and $^{31}P-^{31}P$ COSY NMR spectrum of **3**, DMSO-d_6, 298 K (bottom).

Two of these groups presumably correspond to the symmetrical nonsolvated (**A**) and DMSO solvated (**B**) $[AuAg_2(dppm)_2]^{3+}$ ions; simulations of the spectra ($A_2X_4Q_2$ systems) together with the corresponding coupling constants are given in Figure S5. The $^{107/109}Ag$ to ^{31}P coupling constants were determined using the JRES NMR experiment (Figure S6). The third group of resonances of a lower intensity is generated by the asymmetric $[Au_2Ag(dppm)_2]^{3+}$ (**C**) species where two low field resonances (34.4 and 32.7 ppm) correspond to the gold-bound phosphorus atoms, whereas the third one (6.4 ppm) displays a typical $^{107/109}Ag$ to ^{31}P coupling pattern and should be assigned to the silver coordinated phosphorus (Figure 6). The difference in the metal core composition of the latter species compared to the stoichiometry of the major forms might be compensated by a probable formation of the complex $[Ag_3(PPP)_2]^{3+}$ and its solvated congeners. A relatively low concentration of these molecules and the number of dynamic processes they are involved in could be the reasons why the corresponding resonances are not detected in the $^{31}P-^{31}P$ NMR spectrum. It is additionally supported by the report of Che et al., where the trisilver cluster $[Ag_3(PPP)_2](ClO_4)_3$ shows broad unresolved signals in ^{31}P NMR spectrum.[7a]

Tetranuclear Complexes 4–7. The homonuclear gold complex **5** in DMSO-d_6 solution displays the ^{31}P NMR spectrum (Figure S3), which consists of two resonances (3:1 intensity ratio) at 32.4 and 31.5 ppm with the multiplet structure typical for the strongly correlated A_2B_6 spin system with an extended network of AA, BB, and AB couplings. This is indicative of the presence of only one form of **5** in solution, which retains the motif found in the solid state (Figure 3). Structurally identical homonuclear silver complex **4** displays the $A_2X_6PQ_3$ pattern in its ^{31}P NMR spectrum (Figure S3), featuring additional $^{107/109}Ag$ to ^{31}P couplings for both resonances of central and lateral phosphorus atoms (Figure S7) that is completely compatible with the solid state structure given in Figure 3.

The structure of the heterometallic complex **7** also remains unchanged in solution, which is evidenced by a well resolved spectroscopic pattern, Figure 7, which can be easily simulated using the coupling network shown in Figure S8.

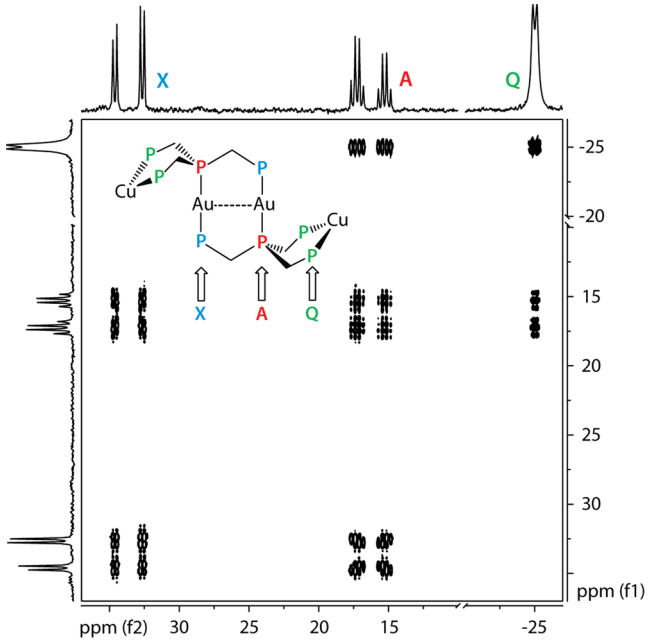

Figure 7. $^{31}P-^{31}P$ COSY NMR spectrum of **7**, DMSO-d_6, 298 K.

Complex **6** is the only tetranuclear complex showing exchange dynamics in DMSO solution, which can be described in terms of metal ion redistribution between two species (Figure 8, top). One of the products of the starting complex conversion is the homonuclear silver complex **4** (indicated as form **B**), which can be easily identified by comparison with the spectrum of individual compound **4**, see Figures 8 and S3 (note that the low-field signal of this compound at 14.9 ppm shown in Figure S3 is omitted for clarity in Figure 8). Another tetranuclear cation formed through the intermolecular metal exchange reaction is the asymmetric $[Au_2Ag_2(PPPP)_2]^{4+}$ molecule (**C**). This species displays two signals of phosphorus atoms bound to gold (34.9 and 31.1 ppm) and a typical $^{107/109}Ag$ splitted multiplet at 0.4 ppm.

These two molecular entities are the minor forms that present in solution; the starting $\{AuAg_3\}$ cation (**A**) dominates in the system to give the strongest signals at 38.2 ppm and −0.5 ppm with a characteristic structure of the $A_2X_6Q_3$ spin system.

dx.doi.org/10.1021/ic500402m | Inorg. Chem. 2014, 53, 4705−4715

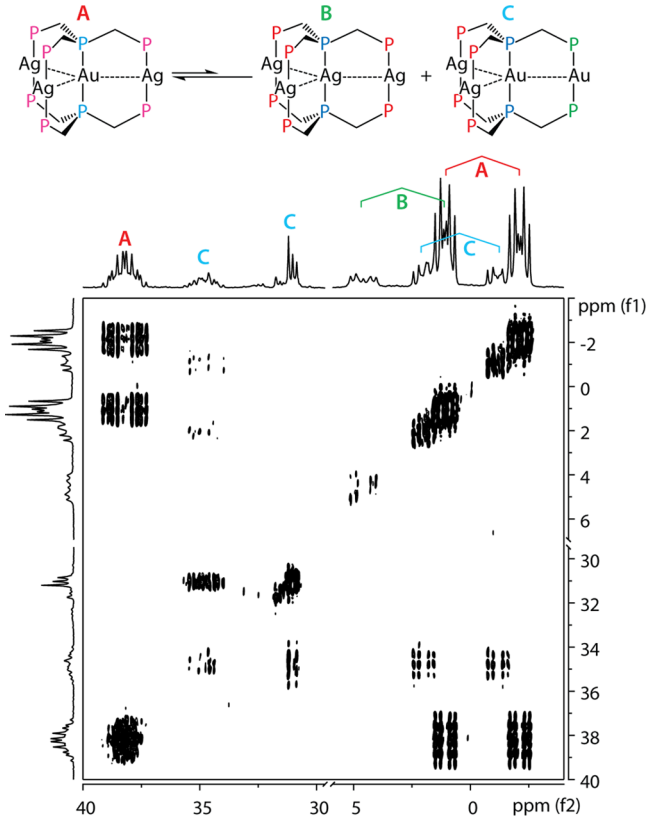

Figure 8. Scheme of the metal ions migration in **6** (top) and $^{31}P-^{31}P$ COSY spectrum of **6**, DMSO-d_6, 298 K (bottom).

Simulation is given in Figure S9; the JRES NMR spectrum is shown in Figure S10.

The proton NMR spectra of **4**, **5**, and **7**, which exist in solution as their unique forms according to the data of ^{31}P NMR spectroscopy, are also compatible with the structural patterns suggested for these polynuclear species, see Experimental and Figures S11, S12.

Solid State Photophysical Properties. The photophysical properties of the complexes under study were investigated in the solid state only due to their complicated solution behavior and are summarized in Table 3. The trinuclear complexes show strong absorption in the near UV region, the position of which depends strongly on the composition of cluster core and ligand sphere (Figure S13). According to the previous studies of the homonuclear $[M_3(PPP)_2L_n]^{m+}$ complexes (M = Au, Ag; *PPP* = dpmp, dcmp),[7b,22,25] their lowest excited state can be assigned to $d_{\sigma^*} \rightarrow p_\sigma$ transitions, d_{σ^*} being a combination of $5d_{z^2}$ orbitals of the trinuclear core, and p_σ consists of $6p_{z^2}$ orbitals of the gold atoms with some admixture of phosphine orbitals of the same symmetry. Not surprisingly, absorption maxima of these compounds substantially depend on the nature of metal coordinated ligands L varying in solution from 326 nm (L_n = $(NCMe)_n$)[22] to 345 nm for Cl^-[26] and 356 nm for $(Cl)_2^{2-}$.[25] In solid the state, the spectroscopic characteristics span an even wider range to show a very strong effect of the counterion, particularly for potentially coordinating anions. For example, the emission maxima of the $[Au_3(dcpm)_2]X_3$ complexes vary from 572 nm (X = SCN) and 558 nm (X = Cl) to 443 nm (X = OTf) and 442 nm (X = PF_6) and also demonstrate considerably different excited state lifetimes: 5.1, 6.4, 2.9, and 2.8 μs, respectively.[7b]

The low energy absorbance maximum of the here studied $[Au_3(PPP)_2]^{3+}$ (**1**) solid state sample (Table 3) appears at 392 nm. For a couple of heterometallic $\{AuCu_2\}$ (**2**) and $\{AuAg_2\}$ (**3a**) clusters, solid state samples display shorter wavelength absorption bands at 355 and 333 nm, respectively. The red shift of absorbance of **2** compared to **3a** can be partly assigned to the higher ground state energy of the d_{σ^*} molecular orbitals composed of gold and copper vs gold and silver orbitals. This observation is completely in line with the assignment of these bands given above and the results of the computational studies, *vide infra*.

In the solid state, the trinuclear complexes are relatively strong emitters (Φ_{em} ranges from 24 to 64%) with the excited state lifetime in the microsecond domain (from 2.2 to 19.3 μs), which points to triplet character of the observed luminescence. The emission spectra of **1**–**3** and **5**–**7** are shown in Figure 9. The gold–silver complex **3b** displays double exponential decay that can be explained by the disorder of the local metal core environment either due to the presence of residual weakly coordinated solvent in the crystalline sample (see for example[27]) or because of variation in the disposition of the counterions around the cationic coordination centers that may result in the presence of two different deactivation pathways of the triplet excited states. The gold–copper complex **2** expectedly shows the lowest energy emission maximum because it has the highest ground state energy (see above) compared to its relatives **1** and **3**. However, the homonuclear $\{Au_3\}$ and $\{AuAg_2\}$ congeners do not display a substantial difference in emission energy very probably due to similar shifts of both triplet excited and singlet ground states.

Structurally related tetrametallic clusters **4**–**6** display very different photophysical behavior. The homonuclear silver complex **4** is not emissive either in solution or in the solid state. On the contrary, its gold relative (**5**) is a rather strong luminophore (Φ_{em} 30%) to give double exponential decay, both exponents of which (6.4 and 3.0 μs) fall into the microsecond domain. A resembling behavior was also found for the heteronuclear $\{AuAg_3\}$ analogue **6**, showing visibly smaller quantum yield (16%) and lower values of double exponential lifetimes (1.8 and 0.6 μs). Taking into account "generally similar" structural motifs of **1**–**3** and **5** and **6**, with the extensive network of metallophilic interactions inside the cluster core, it seems reasonable to assign the phosphorescence of the latter complexes to emission from the triplet excited state followed by

Table 3. Photophysical Properties of 1–3, 5–7 in Solid State, 298 K[a]

	λ_{abs}, nm	λ_{ex}, nm	λ_{em}, nm	τ_{obs}, μs	Φ, %
1	313sh, 392	330 sh, 365, 400sh	460	2.4 ± 0.1	64
2	355	340sh, 380	515	19.3 ± 0.2	30
3a	333	315sh, 380	450	2.0 ± 0.2 (0.72), 0.6 ± 0.1(1.0)	20
3b	325	310sh, 370	455	2.2 ± 0.2 (0.94), 4.8 ± 0.1(1.0)	24
5	351	330sh 390,	460, 550sh	6.4 ± 0.2 (0.62), 3.0 ± 0.1 (1.0)	30
6	332	340sh, 365	450	1.8 ± 0.2 (0.46), 0.6 ± 0.1(1.0)	16
7	328	335, 365	563	0.7 ± 0.1(0.75), 0.4 ± 0.1 (1.0)	6

[a]Relative contribution of each exponent into double exponential decays are given in parentheses.

dx.doi.org/10.1021/ic500402m | *Inorg. Chem.* 2014, 53, 4705–4715

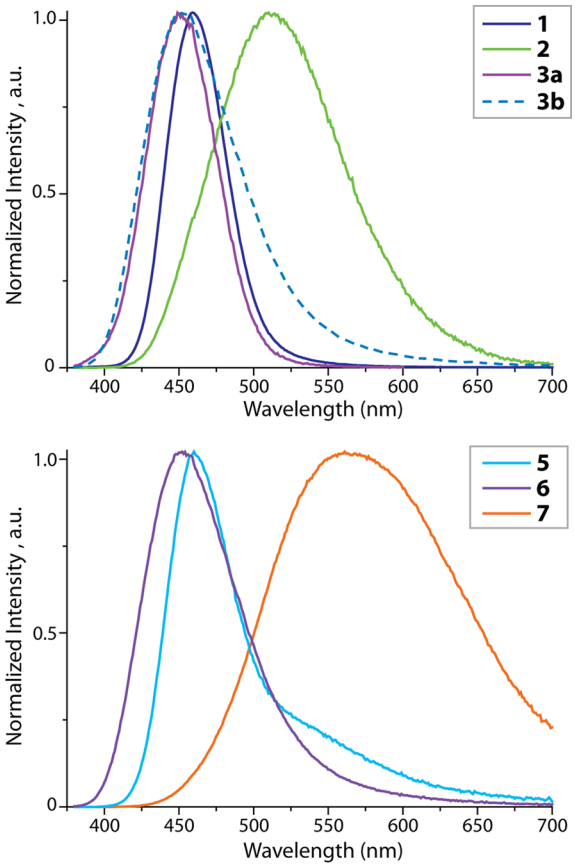

Figure 9. Normalized emission spectra of **1**–**3** and **5**–**7** in the solid state, 298 K.

the $d_{\sigma^*} \rightarrow p_\sigma$ transition facilitated by a strong heavy atom effect of the polynuclear cluster core.

The structure of **7** is essentially different from that of the **4**–**6** family, first of all, due to lower nuclearity of the central {Au–Au} core and the presence of lateral copper ions, which are not directly bonded to the digold center. It is interesting that experimental[24,28] and theoretical[7b] studies of the dinuclear $[Au_2(dcpm)_2]^{2+}$ complexes showed that the solid state photophysics of these lower nuclearity compounds is determined by essentially similar electronic transitions and characterized by substantially higher HOMO–LUMO and LSOMO-HSOMO gaps that result in a blue shift of both the absorption and emission bands compared to the tri- and tetranuclear congeners. In contrast to this observation, complex **7** displays a considerable red shift of emission maximum compared to the **1**–**3** and **5** and **6** series that is a result of the more complicated character of the orbitals taking part in excitation and emission (see below). These molecular orbitals contain the components of both gold and copper metal centers together with an admixture of antibonding orbitals of the phosphine ligands. The presence of double exponential decay in the emission of solid state samples **5**–**7** can be justified by similar reasons to those in the case of complex **3b**.

Computational Results. We carried out quantum chemical calculations at the DFT-PBE0 level of theory to elucidate the photophysical properties of the clusters **1**–**7**. We first optimized the geometries of the studied complexes, after which we carried out time-dependent DFT (TD-DFT) calculations to characterize the lowest energy singlet and triplet excited states (see Experimental Sections for full computational details). The optimized geometries are in line with the solid state X-ray structures even though the optimizations were carried in the gas phase (for all clusters, the essential M–M distances differ less than 0.1 Å in the experimental and theoretical geometries). All optimized geometries in the S_0 ground state are included as Supporting Information.

The wavelengths predicted for the $S_0 \rightarrow S_1$ and $T_1 \rightarrow S_0$ transitions are listed in Table 4, and the corresponding excited states are visualized in Figure 10 for complexes **1**, **5**, and **7** (electron density difference plots for the other clusters and additional molecular orbital plots are illustrated in the Supporting Information, Figures S14, S15). The relative trend of the $T_1 \rightarrow S_0$ emission wavelengths is reproduced very well by the TD-DFT calculations, clusters **2** and **7** showing the longest emission wavelengths. During the structural optimization of the T_1 states, the M–M distances decrease clearly, indicating the metal-centered nature of the transition. For example, in the case of complex **1**, the Au–Au distances decrease from 3.00 to 2.76 Å. For the trinuclear complexes **1**–**3** and tetranuclear complexes **5** and **6**, the $T_1 \rightarrow S_0$ transition is very clearly metal-centered with minor contributions from the phosphine ligands. For cluster **7**, the $T_1 \rightarrow S_0$ transition is different from the other clusters, being rather delocalized over the whole molecule.

Table 4. Computational Photophysical Results for the Clusters 1–7 (PBE0 TD-DFT)

	λ_{ab} $S_0 \rightarrow S_1$ (nm)		λ_{em} $T_1 \rightarrow S_0$ (nm)	
	theor.[a]	expt.	theor.	expt.
1	328 (0.72)	392	458	460
2	360 (0.64)	355	481	515
3a	339 (0.60)	333	446	450
3b	349 (0.58)	325	457	455
5	355 (0.19)	351	441	460
6	365 (0.16)	332	446	450
7	392 (0.003)	328	578	563

[a]Wavelenghts in nm, oscillator strengths given in parentheses.

CONCLUSION

Herein, we reported on the synthesis of the tri- and tetranuclear homo- and heterometallic coinage metal complexes supported by the polydentate phosphine ligands. Using the triphosphine bis(diphenylphosphinomethyl)phenylphosphine, *PPP*, the isostructural linear trimetallic clusters of general formula $[AuM_2(PPP)_2]^+$ (M = Au (**1**), Cu (**2**), Ag (**3**)) were isolated. The tetraphosphine tris(diphenylphosphinomethyl)phosphine, *PPPP*, allowed for the preparation of the star-shaped homometallic compounds $[M_4(PPPP)_2]^{4+}$ (M = Ag (**4**), Au (**5**)) and their mixed-metal congener $[AuAg_3(PPPP)_2]^{4+}$ (**6**). The combination of gold and copper ions in this system, however, resulted in formation of the structurally different complex $[Au_2Cu_2(PPPP)_2(NCMe)_4]^{4+}$ (**7**). The detailed NMR spectroscopic investigation showed that the heterometallic clusters **2**, **3**, and **6** display complicated exchange dynamics in DMSO solution, which can be described in terms of reversible metal ion redistribution between few species and their solvation–desolvation.

The clusters under study except the tetrasilver complex **4** exhibit moderate to strong photoluminescence at room temperature in the solid state with quantum yields from 6%

dx.doi.org/10.1021/ic500402m | Inorg. Chem. 2014, 53, 4705–4715

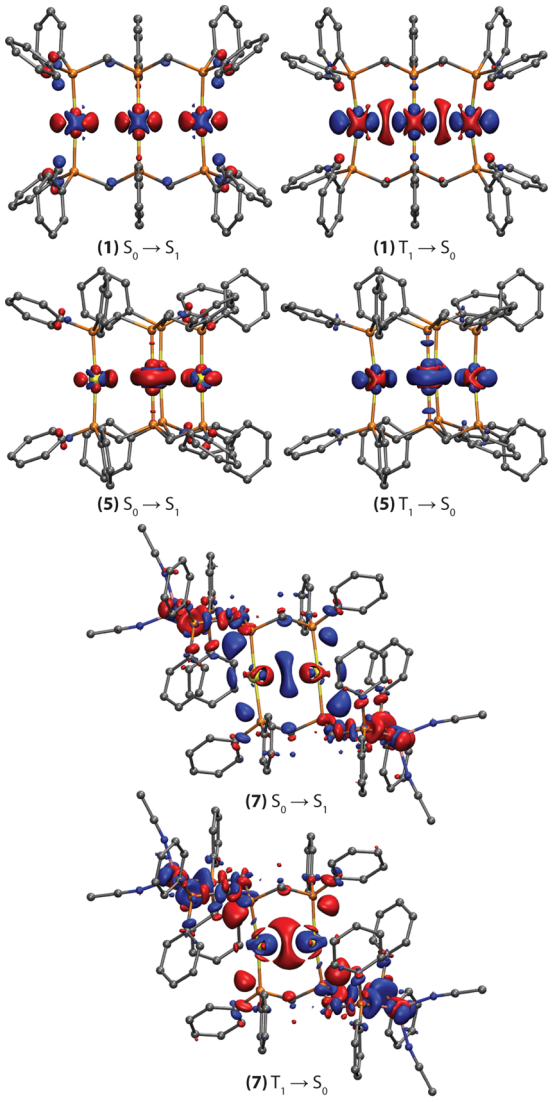

Figure 10. Electron density difference plots for the lowest energy singlet excitation ($S_0 \rightarrow S_1$) and the lowest energy triplet emission ($T_1 \rightarrow S_0$) of the clusters **1**, **5**, and **7** (isovalue 0.002 au). During the electronic transition, the electron density increases in the blue areas and decreases in the red areas. Hydrogen atoms omitted for clarity.

(**7**) to 64% (**1**) and a range of emission energies from 450 (**3a**) to 563 (**7**) nm. Increase of the gold content within the cluster core gradually improves the quantum efficiency of these luminophores in the solid state. The luminescence observed has a triplet origin as the excited state lifetimes were found in the microsecond domain (2.2−19.3 μs).

On the basis of analysis of the absorption, excitation, and emission characteristics for the clusters **1**−**3** and **5**−**7** together with quantum chemical calculations and literature data on the related compounds, the phosphorescence of these complexes can be assigned to the emission from the triplet excited states, determined by the metal cluster-centered $d_{\sigma^*} \rightarrow p_\sigma$ transitions.

■ ASSOCIATED CONTENT

Ⓢ Supporting Information

X-ray crystallographic data in CIF for **1**−**7**, additional NMR spectroscopic data, optimized Cartesian coordinates of the studied systems. This material is available free of charge via the Internet at http://pubs.acs.org.

■ AUTHOR INFORMATION

Corresponding Authors

*E-mail: bird231102@mail.ru.
*E-mail: stunik@inbox.ru.
*E-mail: igor.koshevoy@uef.fi.

Notes

The authors declare no competing financial interest.

■ ACKNOWLEDGMENTS

This research has been supported by the strategic funding of the University of Eastern Finland (Russian−Finnish collaborative project and Spearhead project), the Academy of Finland (grant 268993, I.O.K.), Alfred Kordelin Foundation (A. J. K.), St. Petersburg State University research grant (0.37.169.2014), and grants of the Russian Foundation for Basic Research (14-03-32077). The work was carried out using scientific equipment of the Center of Shared Usage "The analytical center of nano- and biotechnologies of SPbSPU" with financial support of Ministry of Education and Science of Russian Federation. NMR and photophysical studies were performed at the Centre for Magnetic Resonance and at the Center for optical and laser materials research (St. Petersburg State University).

■ REFERENCES

(1) (a) Yam, V. W.-W.; Lo, K. K.-W.; Wong, K. M.-C. *J. Organomet. Chem.* **1999**, *578*, 3−30. (b) Omary, M. A.; Mohamed, A. A.; Rawashdeh-Omary, M. A.; Fackler, J. P. J. *Coord. Chem. Rev.* **2005**, *249*, 1372−1381. (c) Yam, V. W.-W.; Cheng, E. C.-C. *Top. Curr. Chem.* **2007**, *281*, 269−309. (d) López-de-Luzuriaga, J. M., Luminescence of Supramolecular Gold-Containing Materials. In *Modern Supramolecular Gold Chemistry*; Laguna, A., Ed.; Wiley-VCH: Weinheim, Germany, 2008; pp 347−402. (e) Yam, V. W.-W.; Cheng, E. C.-C. *Chem. Soc. Rev.* **2008**, *37*, 1806−1813. (f) Che, C.-M.; Lai, S.-W. Luminescence and Photophysics of Gold Complexes. In *Gold Chemistry*; Mohr, F., Ed.; Wiley-VCH: Weinheim, Germany, 2009; pp 249−282. (g) Chen, Z.-N.; Zhao, N.; Fan, Y.; Ni, J. *Coord. Chem. Rev.* **2009**, *253*, 1−20. (h) Lee, T. K.-M.; Zhu, N.; Yam, V. W.-W. *J. Am. Chem. Soc.* **2010**, *132*, 17646−17648. (i) Lotito, K. J.; Peters, J. C. *Chem. Commun.* **2010**, *46*, 3690−3692. (j) Au, V. K.-M.; Wong, K. M.-C.; Tsang, D. P.-K.; Chan, M.-Y.; Zhu, N.; Yam, V. W.-W. *J. Am. Chem. Soc.* **2010**, *132*, 14273−14278. (k) Yam, V. W.-W.; Wong, K. M.-C. *Chem. Commun.* **2011**, *47*, 11579−11592. (l) Hsu, C.-W.; Lin, C.-C.; Chung, M.-W.; Chi, Y.; Lee, G.-H.; Chou, P.-T.; Chang, C.-H.; Chen, P.-Y. *J. Am. Chem. Soc.* **2011**, *133*, 12085−12099. (m) Hashimoto, M.; Igawa, S.; Yashima, M.; Kawata, I.; Hoshino, M.; Osawa, M. *J. Am. Chem. Soc.* **2011**, *133*, 10348−10351. (n) Takemura, Y.; Nishida, T.; Kure, B.; Nakajima, T.; Iida, M.; Tanase, T. *Chem.—Eur. J.* **2011**, *17*, 10528−10532. (o) Blanco, M. C.; Camara, J.; Gimeno, M. C.; Laguna, A.; James, S. L.; Lagunas, M. C.; Villacampa, M. D. *Angew. Chem., Int. Ed.* **2012**, *51*, 9777−9779. (p) Pei, X.-L.; Yang, Y.; Lei, Z.; Wang, Q.-M. *J. Am. Chem. Soc.* **2013**, *135*, 6435−6437. (q) Visbal, R.; Ospino, I.; Lopez-de-Luzuriaga, J. M.; Laguna, A.; Gimeno, M. C. *J. Am. Chem. Soc.* **2013**, *135*, 4712−4715. (r) To, W.-P.; Chan, K. T.; Tong, G. S. M.; Ma, C.; Kwok, W.-M.; Guan, X.; Low, K.-H.; Che, C.-M. *Angew. Chem., Int. Ed.* **2013**, *52*, 6648−6652. (s) Bergmann, L.; Friedrichs, J.; Mydlak, M.; Baumann, T.; Nieger, M.; Bräse, S. *Chem. Commun.* **2013**, *49*, 6501−6503. (t) Tanase, T.; Otaki, R.; Nishida, T.; Takenaka, H.; Takemura, Y.; Kure, B.; Nakajima, T.; Kitagawa, Y.; Tsubomura, T. *Chem.—Eur. J.* **2014**, *20*, 1577−1596.

(2) (a) Irwin, M. J.; Vittal, J. J.; Puddephatt, R. J. *Organometallics* **1997**, *16*, 3541−3547. (b) Yam, V. W.-W.; Cheng, E. C.-C. *Gold Bull.* **2001**, *34*, 20−23. (c) Yam, V. W.-W.; Wong, K. M.-C. *Top. Curr. Chem.* **2005**, *257*, 1−32. (d) Rawashdeh-Omary, M. A.; Lopez-de-Luzuriaga, J. M.; Rashdan, M. D.; Elbjeirami, O.; Monge, M.; Rodriguez-Castillo, M.; Laguna, A. *J. Am. Chem. Soc.* **2009**, *131*, 3824−

3825. (e) Tiekink, E. R. T.; Kang, J.-G. *Coord. Chem. Rev.* **2009**, *253*, 1627−1648. (f) Lima, J. C.; Rodriguez, L. *Chem. Soc. Rev.* **2011**, *40*, 5442−5456. (g) Liang, J.; Chen, Z.; Yin, J.; Yu, G.-A.; Liu, S. H. *Chem. Commun.* **2013**, *49*, 3567−3569.
(3) (a) Perruchas, S.; Le Goff, X. F.; Maron, S.; Maurin, I.; Guillen, F.; Garcia, A.; Gacoin, T.; Boilot, J.-P. *J. Am. Chem. Soc.* **2010**, *132*, 10967−10969. (b) Koshevoy, I. O.; Lin, C.-L.; Karttunen, A. J.; Haukka, M.; Shih, C.-W.; Chou, P.-T.; Tunik, S. P.; Pakkanen, T. A. *Chem. Commun.* **2011**, *47*, 5533−5535.
(4) (a) Lee, Y.-A.; Eisenberg, R. *J. Am. Chem. Soc.* **2003**, *125*, 7778−7779. (b) Ito, H.; Saito, T.; Oshima, N.; Kitamura, N.; Ishizaka, S.; Hinatsu, Y.; Wakeshima, M.; Kato, M.; Tsuge, K.; Sawamura, M. *J. Am. Chem. Soc.* **2008**, *130*, 10044−10045.
(5) (a) He, X.; Cheng, E. C.-C.; Zhu, N.; Yam, V. W.-W. *Chem. Commun.* **2009**, 4016−4018. (b) Hau, F. K.-W.; He, X.; Lam, W. H.; Yam, V. W.-W. *Chem. Commun.* **2011**, *47*, 8778−8780. (c) He, X.; Yam, V. W.-W. *Coord. Chem. Rev.* **2011**, *255*, 2111−2123. (d) Zhou, Y.-P.; Liu, E.-B.; Wang, J.; Chao, H.-Y. *Inorg. Chem.* **2013**, *52*, 8629−8637.
(6) (a) Strasser, C. E.; Catalano, V. J. *J. Am. Chem. Soc.* **2010**, *132*, 10009−10011. (b) Laguna, A.; Lasanta, T.; Lopez-de-Luzuriaga, J. M.; Monge, M.; Naumov, P.; Olmos, M. E. *J. Am. Chem. Soc.* **2010**, *132*, 456−457. (c) Lasanta, T.; Olmos, M. E.; Laguna, A.; Lopez-de-Luzuriaga, J. M.; Naumov, P. *J. Am. Chem. Soc.* **2011**, *133*, 16358−16361. (d) Koshevoy, I. O.; Chang, Y.-C.; Karttunen, A. J.; Haukka, M.; Pakkanen, T.; Chou, P.-T. *J. Am. Chem. Soc.* **2012**, *134*, 6564−6567. (e) Mo, L.-Q.; Jia, J.-H.; Sun, L.-j.; Wang, Q.-M. *Chem. Commun.* **2012**, *48*, 8691−8693.
(7) (a) Che, C.-M.; Yip, H.-K.; Li, D.; Peng, S.-M.; Lee, G.-H.; Wang, Y.-M.; Liu, S.-T. *J. Chem. Soc., Chem. Commun.* **1991**, 1615−1617. (b) Tong, G. S. M.; Kui, S. C. F.; Chao, H.-Y.; Zhu, N.; Che, C.-M. *Chem.—Eur. J.* **2009**, *15*, 10777−10789.
(8) Campora, J.; Maya, C. M.; Matas, I.; Claasen, B.; Palma, P.; Alvarez, E. *Inorg. Chim. Acta* **2006**, *359*, 3191−3196.
(9) Uson, R.; Laguna, A.; Laguna, M. *Inorg. Synth.* **1989**, *26*, 85−91.
(10) (a) Perdew, J. P.; Burke, K.; Ernzerhof, M. *Phys. Rev. Lett.* **1996**, *77*, 3865−3868. (b) Adamo, C.; Barone, V. *J. Chem. Phys.* **1999**, *110*, 6158−6170.
(11) Weigend, F.; Ahlrichs, R. *Phys. Chem. Chem. Phys.* **2005**, *7*, 3297−3305.
(12) Andrae, D.; Häußermann, U.; Dolg, M.; Stoll, H.; Preuß, H. *Theor. Chem. Acc.* **1990**, *77*, 123−141.
(13) Schäfer, A.; Horn, H.; Ahlrichs, R. *J. Chem. Phys.* **1992**, *97*, 2571−2577.
(14) (a) Furche, F.; Rappoport, D. Density Functional Methods for Excited States: Equilibrium Structure and Electronic Spectra. In *Computational Photochemistry*; Olivucci, M., Ed.; Elsevier: Amsterdam, 2005; pp 93−128. (b) Furche, F.; Ahlrichs, R. *J. Chem. Phys.* **2002**, *117*, 7433−7447. (c) van Wüllen, C. *J. Comput. Chem.* **2011**, *32*, 1195−1201.
(15) Ahlrichs, R.; Bär, M.; Häser, M.; Horn, H.; Kölmel, C. *Chem. Phys. Lett.* **1989**, *162*, 165−169.
(16) *APEX2 - Software Suite for Crystallographic Programs*; Bruker AXS, Inc.: Madison, WI, 2009.
(17) Sheldrick, G. M. *Acta Crystallogr., Sect. A* **2008**, *A64*, 112−122.
(18) Farrugia, L. J. *J. Appl. Crystallogr.* **1999**, *32*, 837−838.
(19) Sheldrick, G. M. *SADABS-2008/1 - Bruker AXS area detector scaling and absorption correction*; Bruker AXS: Madison, WI, 2008.
(20) Spek, A. L. *PLATON, A Multipurpose Crystallographic Tool*; Utrecht University: Utrecht, The Netherlands, 2005.
(21) Nardelli, M. *J. Appl. Crystallogr.* **1999**, *32*, 563−571.
(22) Li, D.; Che, C.-M.; Peng, S.-M.; Liu, S.-T.; Zhou, Z.-Y.; Mak, T. C. W. *J. Chem. Soc., Dalton Trans.* **1993**, 189−194.
(23) (a) Silvestru, C. Gold−Heterometal Interactions and Bonds. In *Modern Supramolecular Gold Chemistry*; Laguna, A., Ed.; Wiley-VCH: Weinheim, Germany, 2008; pp 181−295. (b) Koshevoy, I. O.; Shakirova, J. R.; Melnikov, A. S.; Haukka, M.; Tunik, S. P.; Pakkanen, T. A. *Dalton Trans.* **2011**, *40*, 7927−7933. (c) Hu, T.; Zhao, L.; Mak, T. C. W. *Organometallics* **2012**, *31*, 7539−7547. (d) Schmidbaur, H.; Schier, A. *Chem. Soc. Rev.* **2012**, *41*, 370−412.
(24) King, C.; Wang, J. C.; Khan, M. N. I.; Fackler, J. P. J. *Inorg. Chem.* **1989**, *28*, 2145−2149.
(25) Tanase, T.; Masuda, K.; Matsuo, J.; Hamaguchi, M.; Begum, R. A.; Yano, S. *Inorg. Chim. Acta* **2000**, *299*, 91−99.
(26) Xiao, H.; Weng, Y.-X.; Wong, W.-T.; Mak, T. C. W.; Che, C.-M. *J. Chem. Soc., Dalton Trans.* **1997**, 221−226.
(27) (a) Makal, A.; Benedict, J.; Trzop, E.; Sokolow, J.; Fournier, B.; Chen, Y.; Kalinowski, J. A.; Graber, T.; Henning, R.; Coppens, P. *J. Phys. Chem. A* **2012**, *116*, 3359−3365. (b) Volz, D.; Nieger, M.; Friedrichs, J.; Baumann, T.; Bräse, S. *Langmuir* **2013**, *29*, 3034−3044.
(28) Li, D.; Che, C.-M.; Kwong, H.-L.; Yam, V. W.-W. *J. Chem. Soc., Dalton Trans.* **1992**, 3325−3329.